Search for Slowly Moving Massive Magnetic Monopoles

D. E. Groom, E. C. Loh, H. N. Nelson, and D. M. Ritson

Department of Physics and Stanford Linear Accelerator Center, Stanford University, Stanford, California 94305, and Department of Physics, University of Utah, Salt Lake City, Utah 84112

(2) Monopoles are gravitationally bound to the galaxy, and account for most of the halo mass. This assumption unambiguously implies velocities near $10^{-3}c$ and can be stretched (with difficulty, especially for magnetic field survival) to Cabrera's flux limit.

Mayflower Mine, Utah

The Monopole dL/dx "cutoff" dispute

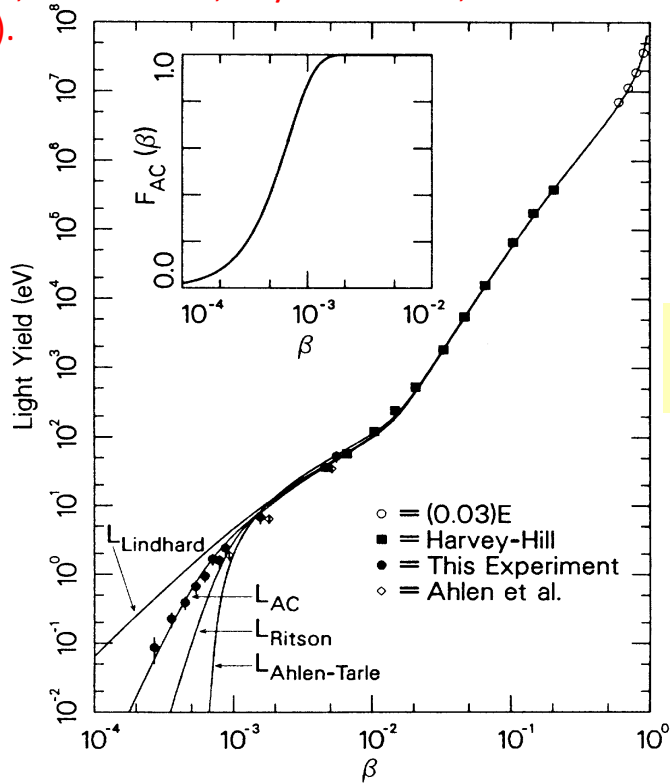D.J.Ficenec, S.P. Ahlen, A.A. Martin, J.A. Musser, and G. Tarle, Phys. Rev. D 36, 311 (1987).

Fig. 2 are two models which have been used in the past to predict the scintillation response to very-low-energy particles. A sharp response threshold occurs in the model of Ahlen-Tarlé[11] at a velocity of $6 \times 10^{-4} c$. The model developed by Ritson[20] to estimate the response of scintillators to monopoles has been modified by us to be appropriate for protons. It is apparent that both of these models were overly conservative in their prediction, of scintillation at low velocities. The best fit for the data is obtained if we modify the Lindhard stopping with an adiabatic correction factor of the form $F_{AC}(\beta) = 1 - \exp(-\beta^2/\beta_0^2)$, where $\beta_0 = 7 \times 10^{-4}$. F_{AC}, which indicates the reduced efficiency for electronic excitation at low velocities, is shown in Fig. 2. The absence of a sharp threshold in F_{AC} is due either to level mixing effects or to high-velocity tails in the electron momenta distributions.

M.E. Rudd, Phys. Rev. A 20, 787 (1987).

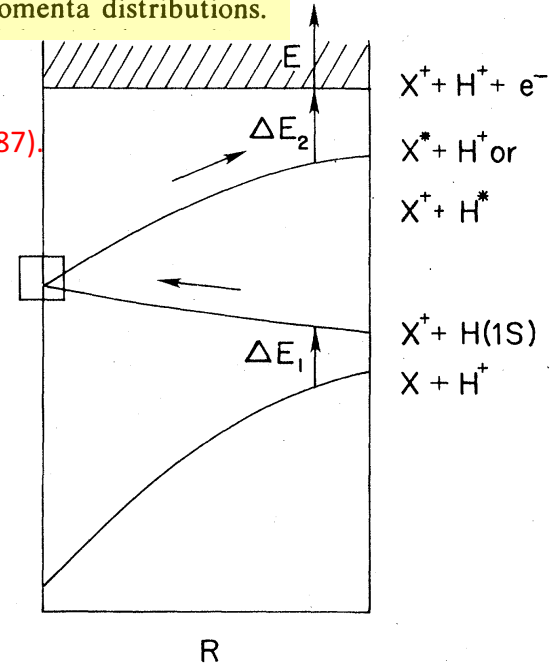FIG. 2. Light yield vs proton velocity for data taken at 2 and 24 keV. See text for explanation of the curves.

FIG. 14. Schematic correlation diagram showing proposed transitions accounting for exponential energy dependence of electron-ejection cross sections on electron energy (see text).

For LXe... issue is the struck xenon atom and the response to **that...**

LUX LXe Charge yield v. kinematic energy

(Brown – Rick G, J. Verbus... UCSB – Carmen Carmona, now Penn St.)
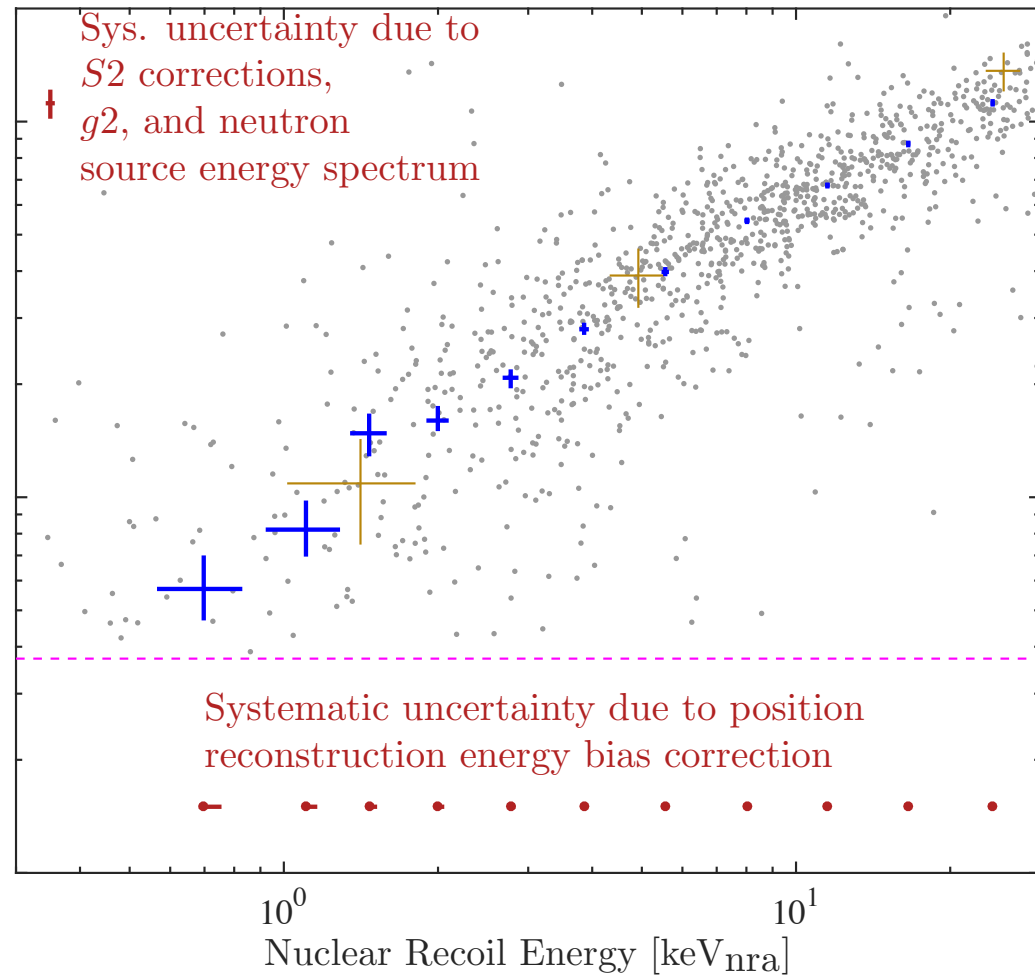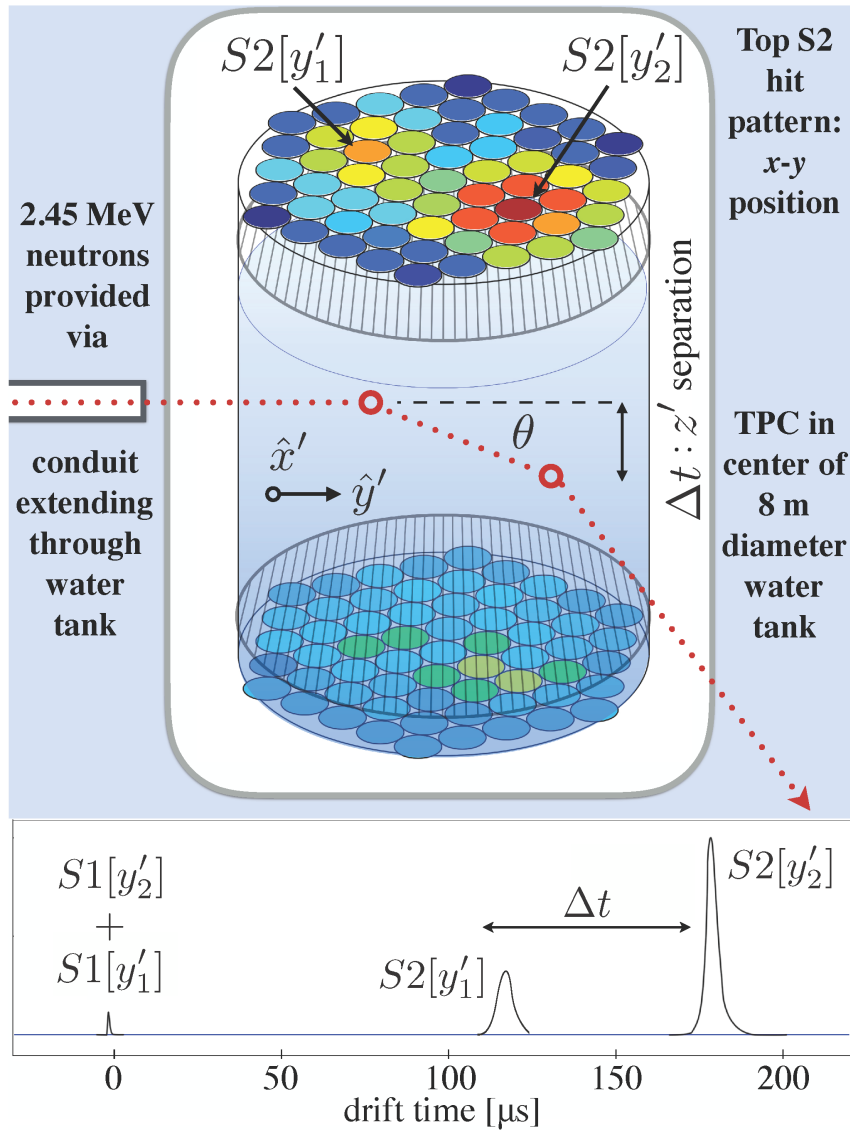
Xenon

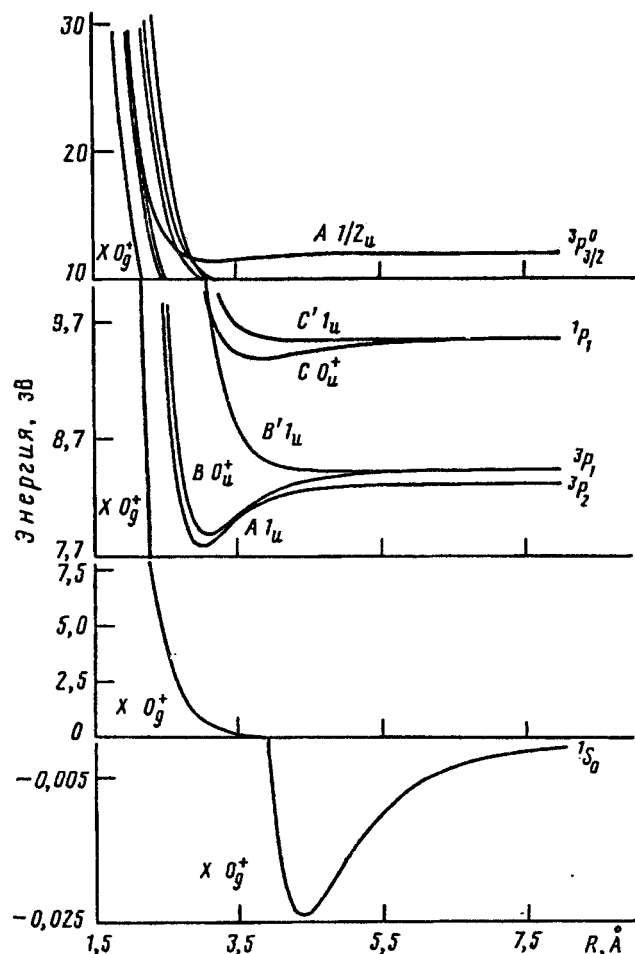I.I.Oleinik and N.M. Kuznetsov,
Khimicheskaya Fizika 12, 1339 (1993)

Рис. 4. Потенциальные кривые Xe₂, Xe₂⁺, рассчитанные с помощью EHFACE2-модели

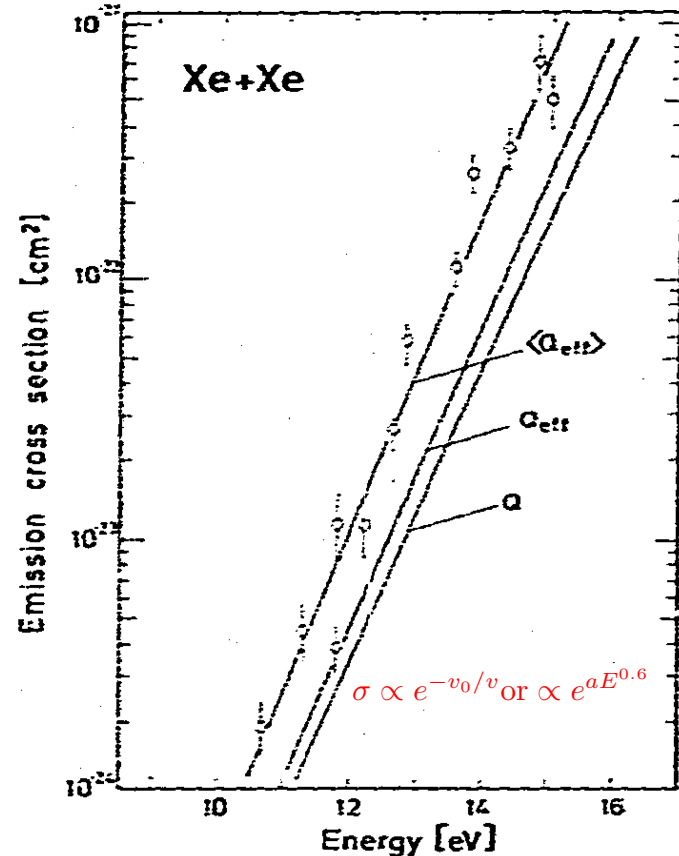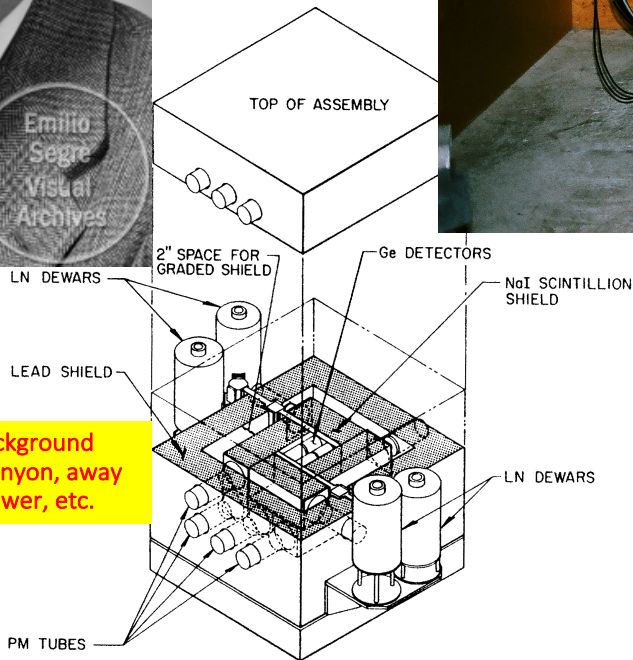$$\sigma \propto e^{-v_0/v} \text{or} \propto e^{aE^{0.6}}$$

Fig. 2. Emission cross section for Xe + Xe collisions as a function of the center-of-mass energy. The solid lines correspond to cross sections given in eq. (3), convoluted with the target motion and primary beam velocity distribution.

David Caldwell
UCSB

Manhattan Project Low Background Counting Facility – Pajarito Canyon, away from radioactivity, noisy power, etc.

TOP OF ASSEMBLY

2" SPACE FOR GRADED SHIELD

LN DEWARS

Ge DETECTORS

NaI SCINTILLION SHIELD

LEAD SHIELD

LN DEWARS

PM TUBES
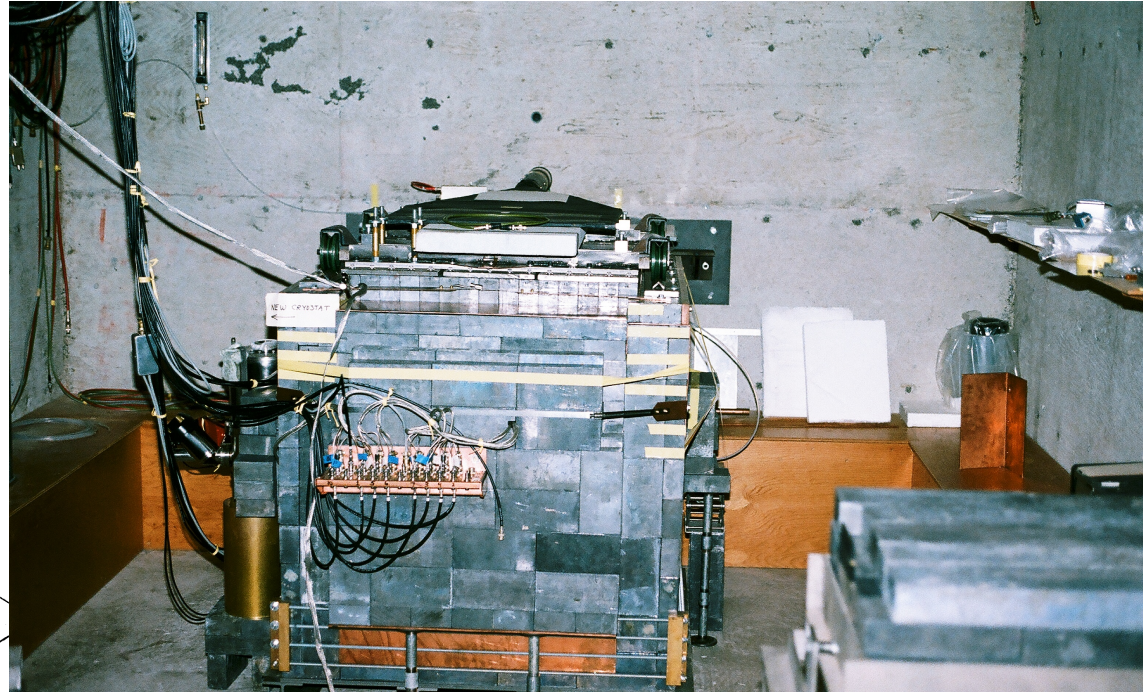
XBL 839-11853

Fig. 1 Exploded view of the complete detector assembly with the upper layer raised.

Backgrounds!!

Back(grounds) to the Future

- Long-lived radioactive chains
- The 3 emanations (Radon, Thoron, Actinon)
- **(alpha,n)**

"Manhattan Projected Low Background Counting Facility – Pajarito Canyon, away from radioactivity, noisy power, etc.
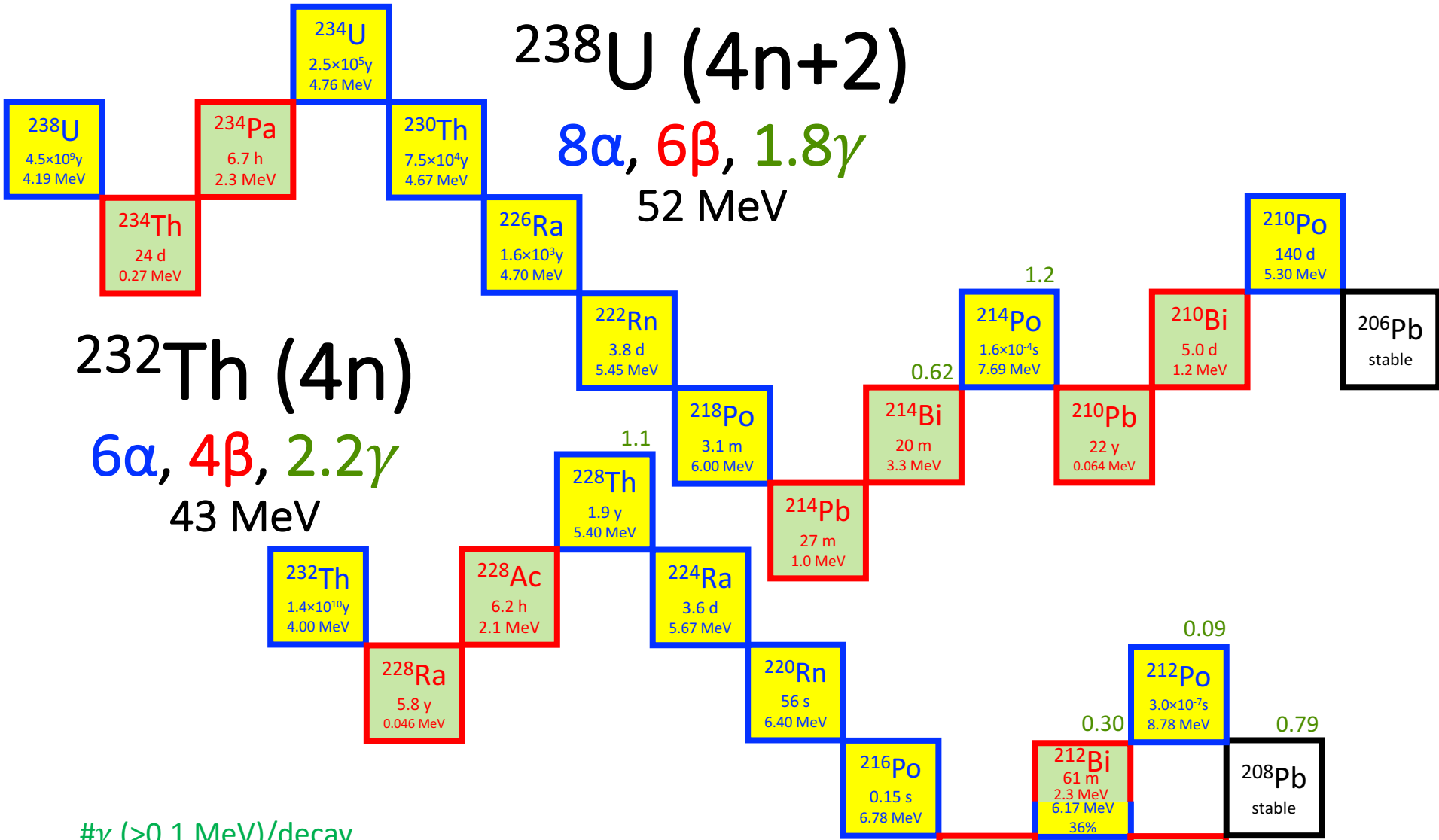
238U (4n+2)

8α, 6β, 1.8γ

52 MeV

232Th (4n)

6α, 4β, 2.2γ

43 MeV

238U
4.5×10⁹y
4.19 MeV

234Th
24 d
0.27 MeV

234Pa
6.7 h
2.3 MeV

234U
2.5×10⁵y
4.76 MeV

230Th
7.5×10⁴y
4.67 MeV

226Ra
1.6×10³y
4.70 MeV

222Rn
3.8 d
5.45 MeV

218Po
3.1 m
6.00 MeV

228Th
1.9 y
5.40 MeV

1.1

232Th
1.4×10¹⁰y
4.00 MeV

228Ac
6.2 h
2.1 MeV

224Ra
3.6 d
5.67 MeV

228Ra
5.8 y
0.046 MeV

220Rn
56 s
6.40 MeV

216Po
0.15 s
6.78 MeV

214Pb
27 m
1.0 MeV

214Bi
20 m
3.3 MeV

0.62

214Po
1.6×10⁻⁴s
7.69 MeV

1.2

210Pb
22 y
0.064 MeV

210Bi
5.0 d
1.2 MeV

210Po
140 d
5.30 MeV

206Pb
stable

212Pb
11 h
0.57 MeV

212Bi
61 m
2.3 MeV
6.17 MeV
36%

0.30

212Po
3.0×10⁻⁷s
8.78 MeV

0.09

208Tl
3.1 m
5.0 MeV

208Pb
stable

0.79

#γ (>0.1 MeV)/decay

α
$\tau_{1/2}$
$\bar{E}_\alpha$

β
$\tau_{1/2}$
Q_β

| 81 ²P°₁/₂ Tl Thallium 204.38* [Hg]6p 6.1083 | 82 ³P₀ Pb Lead 207.2 [Hg]6p² 7.4167 | 83 ⁴S°₃/₂ Bi Bismuth 208.98040 [Hg]6p³ 7.2855 | 84 ³P₂ Po Polonium (209) [Hg]6p⁴ 8.414 | 85 ²P°₃/₂ At Astatine (210) [Hg]6p⁵ 9.3175 | 86 ¹S₀ Rn Radon (222) [Hg]6p⁶ 10.7485 |
| 87 ²S₁/₂ Fr Francium (223) [Rn]7s 4.0727 | 88 ¹S₀ Ra Radium (226) [Rn]7s² 5.2784 | 89 ²D₃/₂ Ac Actinium (227) [Rn]6d7s² 5.3802 | 90 ³F₂ Th Thorium 232.0377 [Rn]6d²7s² 6.3067 | 91 ⁴K₁₁/₂ Pa Protactinium 231.03588 [Rn]5f²6d7s² 5.89 | 92 ⁵L°₆ U Uranium 238.02891 [Rn]5f³6d7s² 6.1941 |

^{235}U (4n+3)

7α, 4β, 2γ

46 MeV

^{239}Pu
2.4×10^4y
5.14 MeV

^{235}U
7.0×10^8y
4.39 MeV

0.85

^{231}Pa
3.3×10^4y
4.97 MeV

0.09

^{227}Th
19 d
5.88 MeV

0.39

^{231}Th
26 h
0.39 MeV

^{227}Ac
22 y
0.045 MeV

^{223}Ra
11 d
5.67 MeV

0.35

^{219}Rn
4.0 s
6.76 MeV

0.17

^{215}Po
1.8×10^{-3}s
7.39 MeV

0.10

^{211}Bi
2.1 m
6.57 MeV

^{207}Pb
stable

^{211}Pb
36 m
1.4 MeV

0.13

^{207}Tl
4.8 m
1.4 MeV

^{241}Am
430 y
5.45 MeV

^{237}Np
2.1×10^6y
4.77 MeV

0.16

^{233}U
1.6×10^5y
4.82 MeV

0.02

^{233}Pa
27 d
0.57 MeV

^{229}Th
7.9×10^3y
4.87 MeV

0.24

^{225}Ac
10 d
5.79 MeV

0.13

^{225}Ra
15 d
0.36 MeV

^{221}Fr
4.8 m
6.31 MeV

0.12

^{217}At
3.2×10^{-2}s
7.07 MeV

0.27

^{213}Po
3.7×10^{-6}s
8.38 MeV

^{209}Bi
stable

^{213}Bi
46 m
1.4 MeV

^{209}Pb
3.2 h
0.64 MeV

^{237}Np (4n+1)

7α, 4β, 0.8γ

67 MeV

#γ (>0.1 MeV)/decay

α
$\tau_{1/2}$
$\bar{E}_\alpha$

β
$\tau_{1/2}$
Q_β

81 $^2P^\circ_{1/2}$	82 $^3P_0$	83 $^4S^\circ_{3/2}$	84 $^3P_2$	85 $^2P^\circ_{3/2}$	86 $^1S_0$
Tl	**Pb**	**Bi**	**Po**	**At**	**Rn**
Thallium	Lead	Bismuth	Polonium	Astatine	Radon
204.38*	207.2	208.98040	(209)	(210)	(222)
[Hg]6p	[Hg]6p^2	[Hg]6p^3	[Hg]6p^4	[Hg]6p^5	[Hg]6p^6
6.1083	7.4167	7.2855	8.414	9.3175	10.7485

87 $^2S_{1/2}$	88 $^1S_0$	89 $^2D_{3/2}$	90 $^3F_2$	91 $^4K_{11/2}$	92 $^5L^\circ_6$	93 $^6L_{11/2}$	94 $^7F_0$	95 $^8S^\circ_{7/2}$
Fr	**Ra**	**Ac**	**Th**	**Pa**	**U**	**Np**	**Pu**	**Am**
Francium	Radium	Actinium	Thorium	Protactinium	Uranium	Neptunium	Plutonium	Americium
(223)	(226)	(227)	232.0377	231.03588	238.02891	(237)	(244)	(243)
[Rn]7s	[Rn]7s^2	[Rn]6d7s^2	[Rn]6d^{2}7s^2	[Rn]5f^{2}6d7s^2	[Rn]5f^{3}6d7s^2	[Rn]5f^{4}6d7s^2	[Rn]5f^{6}7s^2	[Rn]5f^{7}7s^2
4.0727	5.2784	5.3802	6.3067	5.89	6.1941	6.2655	6.0258	5.9738

Bernard Sadoulet

II Rate and Backgrounds ⟹ Signatures

Unfortunately : - lower limit of rates < <   3° exchange
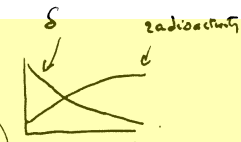
- for $\gamma^K \gamma 5$ coupling $S(S+1)$ coupling

2 problems

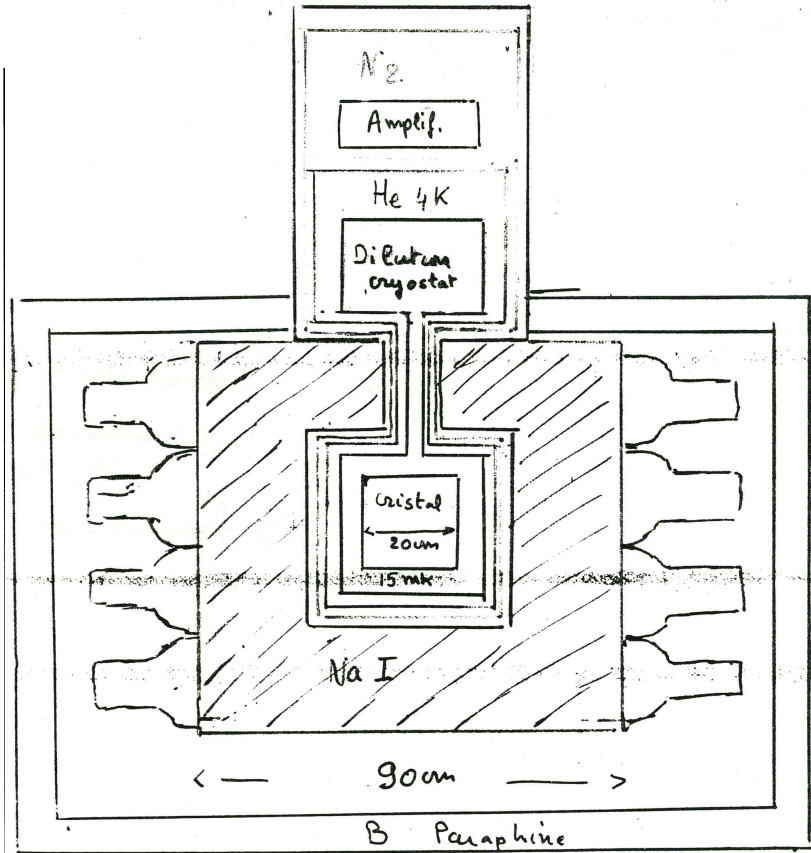□ Sensitivity. ⟸ low energy depositions

should be able to detect   ~ 100 eV

□ No spurious counts

← Detector
Radioactive background

Signatures

□ Shape of spectrum

inject some radioactivity and
check that no peak

Schematics of
bolometic detector

Is it necessary?

- lead shielding?
- Go to a mine?

LOW TEMPERATURE DETECTORS FOR
NEUTRINO EXPERIMENTS AND DARK MATTER SEARCHES

B. Cabrera

Physics Department, Stanford University, Stanford, California 94305

D. Caldwell

Physics Department, UC Santa Barbara, Santa Barbara, California

and B. Sadoulet

Physics Department, UC Berkeley, Berkeley, California 94720

Abstract

We summarize the research efforts to build a new class of particle detectors based on phonon propagation in insulating crystals, such as silicon, and quasiparticle propagation in superconductors. Such detectors in the 1 kilogram mass range would be used for neutrino experiments, neutrinoless double beta decay experiments and dark matter searches.

Introduction

During the last decade, innovative experiments have addressed some of the most interesting questions in particle physics and at the interface between particle physics and astrophysics. These include searches for a finite neutrino mass through double beta decay, neutrino oscillations and tritium end point experiments, as well as searches for elementary particle candidates for dark matter such as magnetic monopoles, massive neutrinos, photinos and axions.

We now believe that substantially more sensitive searches can be mounted which utilize the properties of superconductors and insulating crystals at temperatures below 1 K. The diverse motivations for developing these detectors have come from ideas for improved neutrino experiments (Stanford group), form ideas for dark matter searches for candidates which are weakly interacting massive particles (LBL/UC Berkeley group), and from ideas for the next generation of double beta decay experiments (UC Santa Barbara group). Our three groups have started the development of such detectors in the kilogram mass range. Their properties should include thresholds as low as a hundred electron volts, resolution at least an order of magnitude better than semiconductor detectors and very low radioactive backgrounds. In this paper, we summarize these research efforts.

1 NEUTRINO PHYSICS

Among these new areas of research would be low-energy neutrino detection by means of coherent elastic scattering from nuclei via the neutral weak current. This process, as yet undetected but theoretically firmly based, gives the largest possible interaction rates for a neutrino detector, but results in extremely small energy transfers to the detector (~1-10 keV) [1]. Such energy transfers should be easily detected only by the cryogenic schemes described in Sec 4, such as the silicon crystal acoustic detectors (SiCADs) [2]. Neutrino-electron scattering could also be detected in such devices. The combination of these two processes makes self-normalizing neutrino oscillation experiments possible and provides sensitivity to smaller neutrino masses.

SiCADs would be sensitive to the purely neutral-current process of coherent elastic scattering from nuclei, as well as the mixed charged-plus-neutral-current process of neutrino scattering from electrons. In the Standard Model, the neutral-current cross section is independent of the neutrino's leptonic flavor, while the charged current cross section is dependent upon the neutrino flavor. The two processes can be experimentally distinguished by their very different energy depositions in the detector. For a reactor neutrino energy spectrum, the coherent scattering from nuclei deposits the nuclear recoil energy in the SiCAD, at most ~8 keV at the highest rector neutrino energies. The differential cross sections as a function of recoil energy are shown in Fig 1 for a reactor neutrino spectrum. Scattering from the much lighter electrons results in transfer of an appreciable fraction of the neutrino energy, 0.5-10 MeV. Due to the kinematics, a monochromatic neutrino spectrum gives rise to roughly a step-function energy deposition spectrum for both processes, extending from zero to the maximum energy transfers mentioned above.

1.1 Reactor Neutrinos

Nuclear reactors are a source of electron antineutrinos with energies from 0.25 to 10 MeV, and fluxes as high as ~10^{13} cm^{-2} s^{-1} at the detector. Coherent scattering events with recoil energy >1 keV occur in silicon at a rate of about 100 kg^{-1} day^{-1}, several orders of magnitude greater than rates in present neutrino detectors [1,3]. The coherent scattering process is important in the dynamics of energy transfer in supernovae, but it has never been observed in the lab. A SiCAD with low-energy background count rate equal to that currently achieved in above-ground double-beta decay experiments using Ge semiconductor diode detectors, would permit a measurement of the coherent scattering with a signal to background ratio of exceeding unity (see Ref 3 for a more detailed consideration of backgrounds in a reactor neutrino experiment).

Scattering of reactor neutrinos from electrons in silicon occurs at a rate of about 4 kg^{-1} day^{-1}. Detection of these recoil electrons would permit a small, movable detector to be sensitive to neutrino oscillations. The dominant charged current scattering process is allowed only for electron-type neutrinos. Oscillations would therefore result in a reduced rate of neutrino-electron scattering events, and also a change in the energy dependence of the upper part of the recoil energy spectrum (see Fig 1). The low neutrino energy threshold of the acoustic detector would permit sensitivity to lower values of Δm^2 than in current experiments, perhaps as low as 10^{-4} (eV/c^2)^2. The flavor-independent coherent nuclear elastic scattering process simultaneously provides an oscillation-independent normalization of the total incident antineutrino flux.
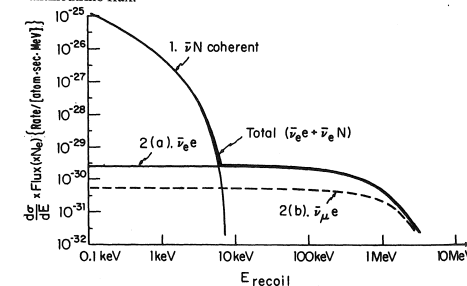

Fig 1.   Differential cross section versus recoil energy for elastic scattering of neutrinos off of Si nuclei and electrons for reactor flux and spectrum.

Laboratory Limits on Galactic Cold Dark Matter

D. O. Caldwell, R. M. Eisberg, D. M. Grumm, and M. S. Witherell

Department of Physics, University of California, Santa Barbara, California 93106

B. Sadoulet

Physics Department, University of California, Berkeley, California 94720

and

F. S. Goulding and A. R. Smith

Lawrence Berkeley Laboratory, Berkeley, California 94720
(Received 13 November 1987; revised manuscript received 16 May 1988)
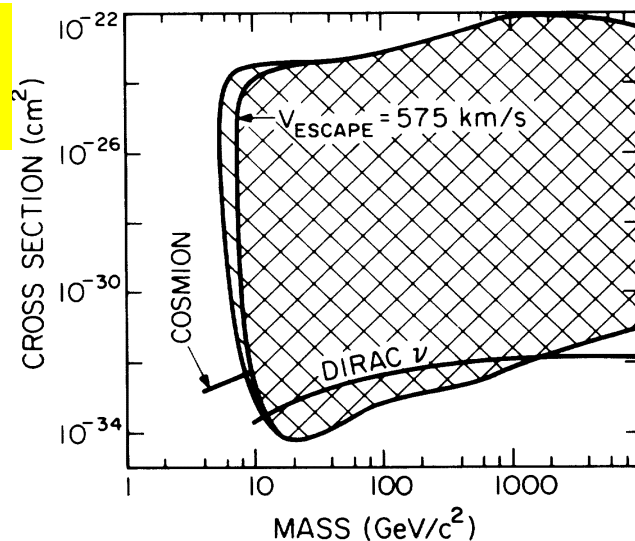
Oroville

Not per nucleon

FIG. 2. Mass exclusion plot for particular cross sections for the interaction with Ge (or, for the upper boundary, with the Earth) using data from the present experiment. The larger shaded region is excluded if the escape velocity is infinite; the smaller region, if the escape velocity is 575 km/s. All limits are 2σ. The curve near the bottom of the plot shows the cross section as a function of mass for a Dirac neutrino. The short line with the label cosmion shows the expected cross section for cosmions with mass between 4 and 9 GeV/c^2.
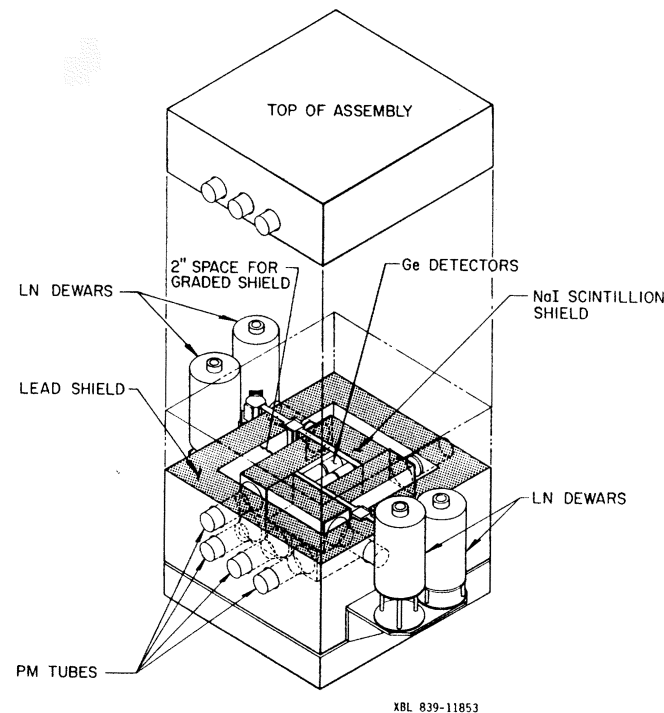

Fig. 1 Exploded view of the complete detector assembly with the upper layer raised.

Vector Coupling
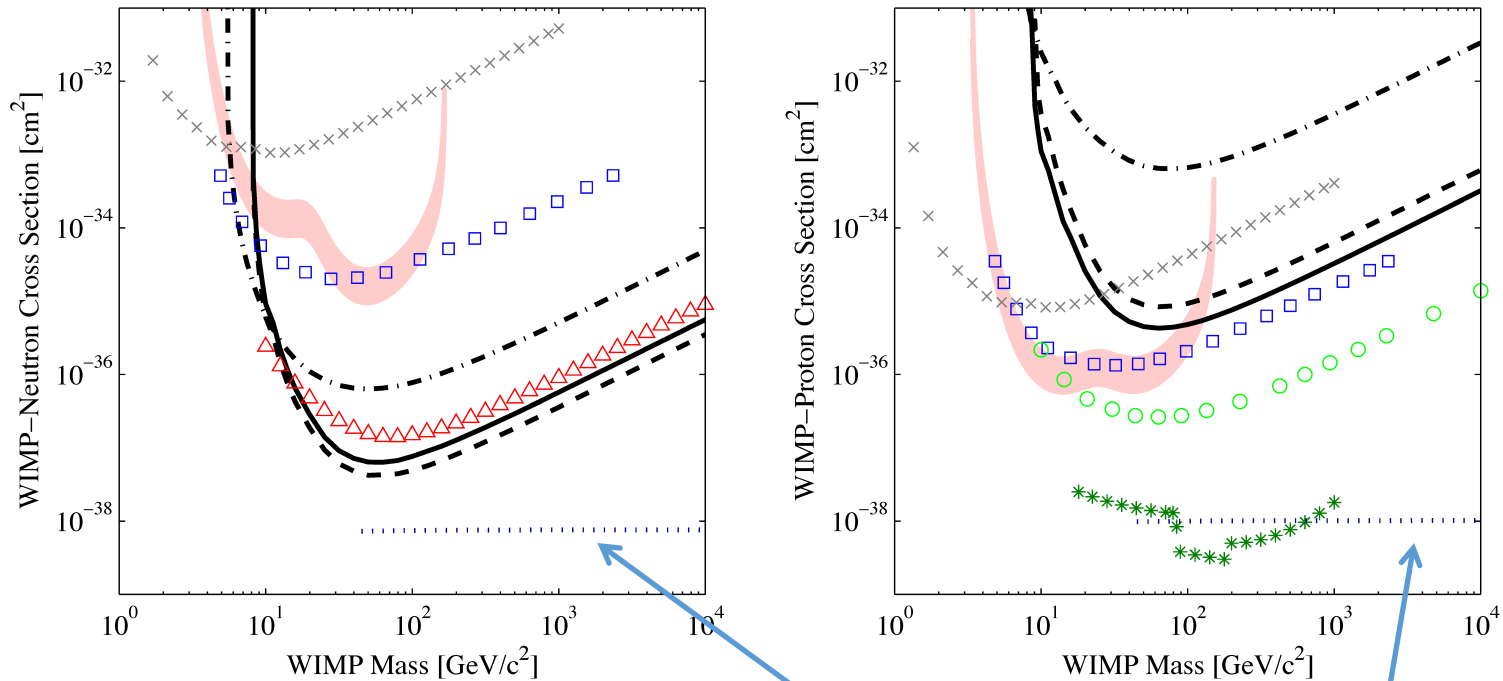K. Greist/Scalar/Higgs - Later

FIG. 1: Upper limit contours (90% confidence level) for recent CDMS data sets, plotted in the cases of (*left*) pure neutron and (*right*) pure proton coupling. We show limits based on Ge (solid) and Si (dash-dot) from the combined Soudan data (black). Dashed curves represent Ge limits using the alternate form factor from [15]. As benchmarks, we also include interpretations of the DAMA/NaI annual modulation signal [10] (filled regions are 3σ-allowed) and limits from other leading experiments: CRESST I [16] as computed in [11] ("×"s), PICASSO [17] (squares), NAIAD [18] (circles), ZEPLIN I [19] (triangles), and Super-Kamiokande [20] (asterisks; an indirect search, based on different assumptions). EDELWEISS [21] and SIMPLE [22] report limits (not shown for clarity) comparable to CDMS Si and PICASSO, respectively. As a theoretical benchmark (see text), horizontal dotted lines indicate expected cross sections for a heavy Majorana neutrino. Plots courtesy of [23].
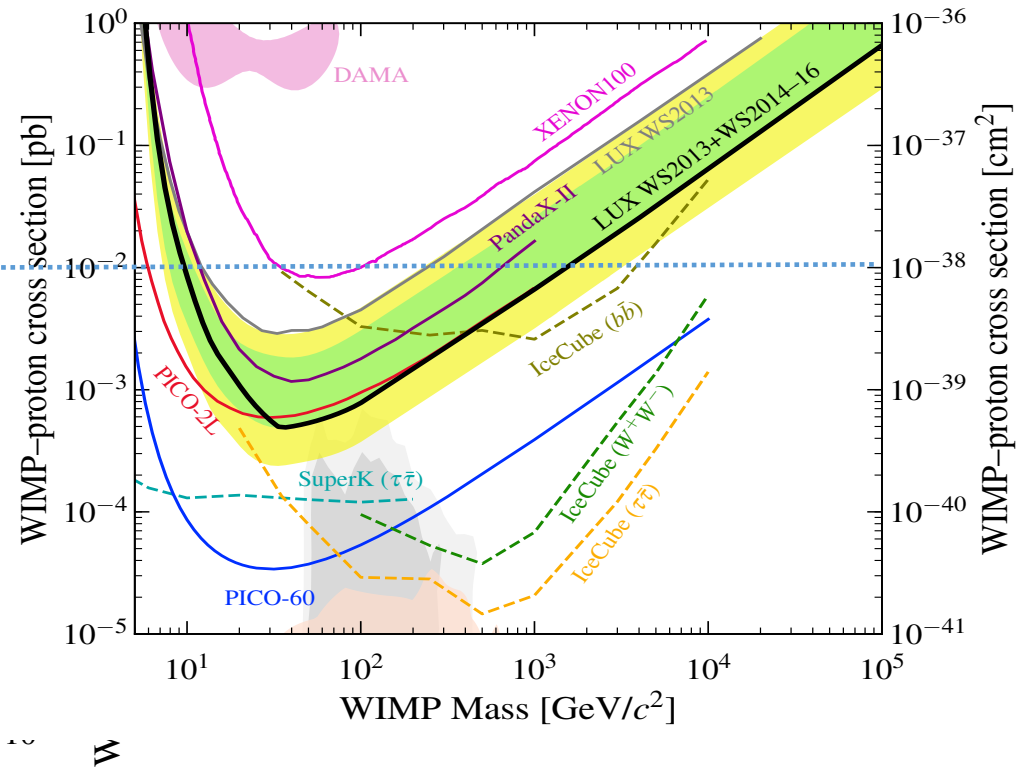
Axial/Spin Dependent Coupling

Tangent - More recent plot (2017)

Neutron
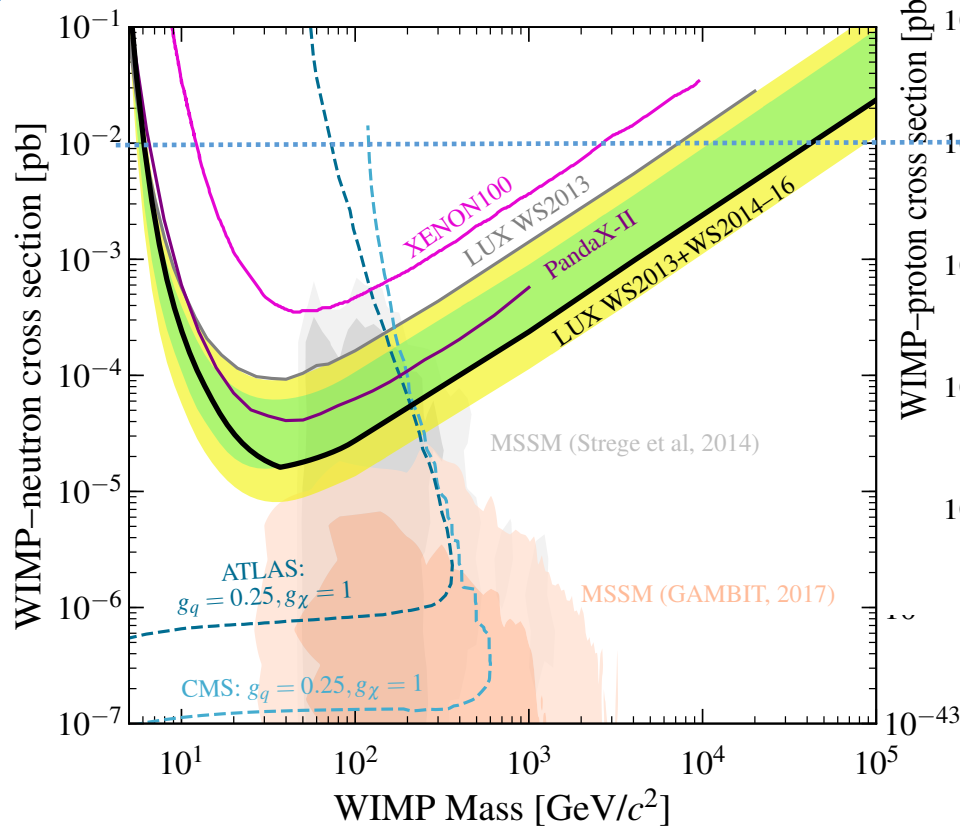
Proton

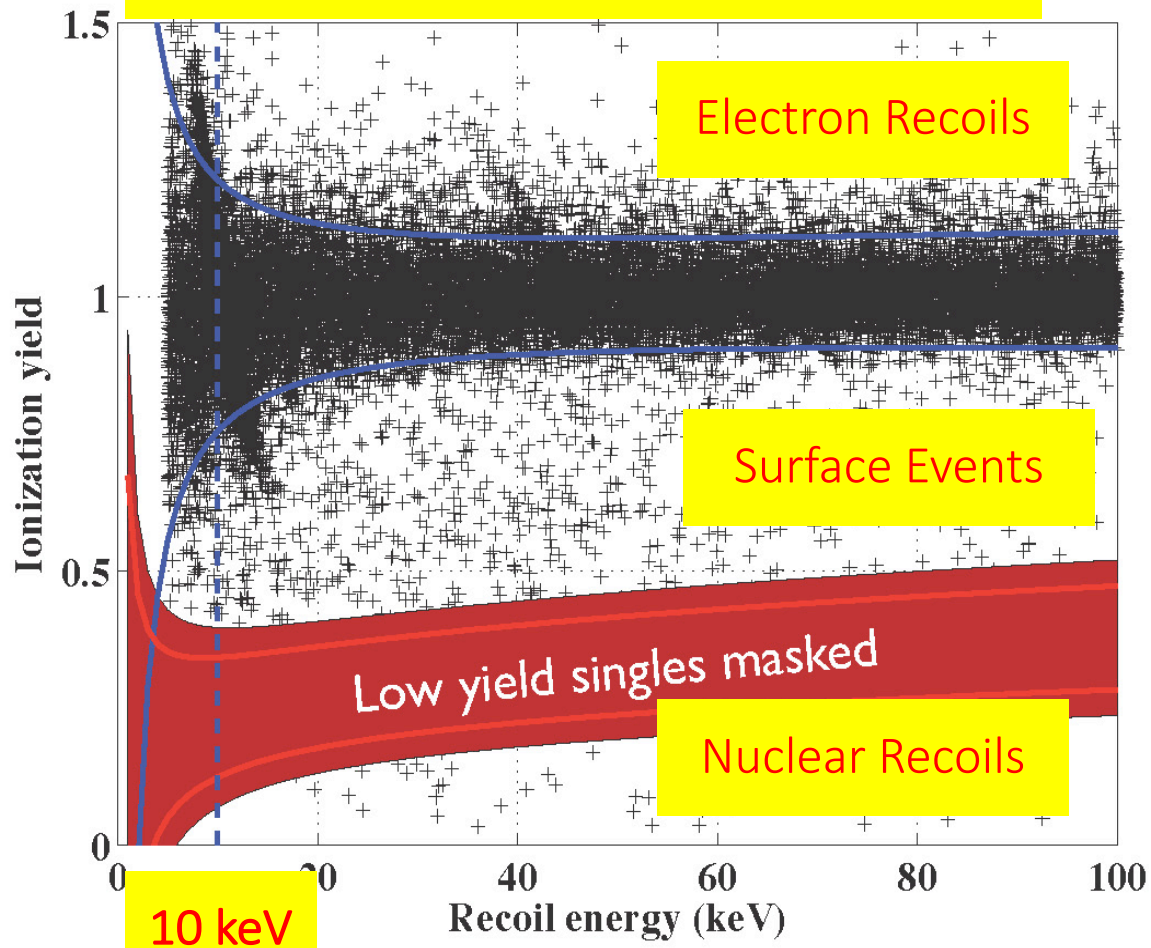# Xenon – best for generalized EFT couplings, except proton-specific (PICO)

Compare… Argon

- 9 `stable' isotopes
- 2 with unpaired neutron
- Would love to deplete ^{136}Xe

^{A}Z	$\tau_{\frac{1}{2}}$ or f	J^p
^{122}Xe	20 h	0$^+$
^{123}Xe	2.1 h	(1/2)$^+$
^{124}Xe	0.10 %	0$^+$
^{125}Xe	17 h	(1/2)$^+$
^{126}Xe	0.09 %	0$^+$
^{127}Xe	**36 d**	**(1/2)$^+$**
^{128}Xe	1.91 %	0$^+$
^{129}Xe	**26.4 %**	**(1/2)$^+$**
^{130}Xe	4.1 %	0$^+$
^{131}Xe	**21.2 %**	**(3/2)$^+$**
^{132}Xe	26.9 %	0$^+$
^{133}Xe	5.2 d	(3/2)$^+$
^{134}Xe	10.4 %	0$^+$
^{135}Xe	9.1 h	(3/2)$^+$
^{136}Xe	8.9 % (2.2×10^{21} y)	0$^+$

God made the bulk; the devil sneaked the surfaces in

CDMS-II (2009) - Soudan

Electron Recoils

Surface Events

Low yield singles masked

Nuclear Recoils

10 keV

Sanford U.R.F. Lead, South Dakota

Sanford Underground Research Facility

Davis Cavern 1480 m
(4200 mwe)
LUX Water Tank

LUX/LZ
Here

LZ – Less Zagan

Existing water tank

Gd-loaded scintillator outer detector
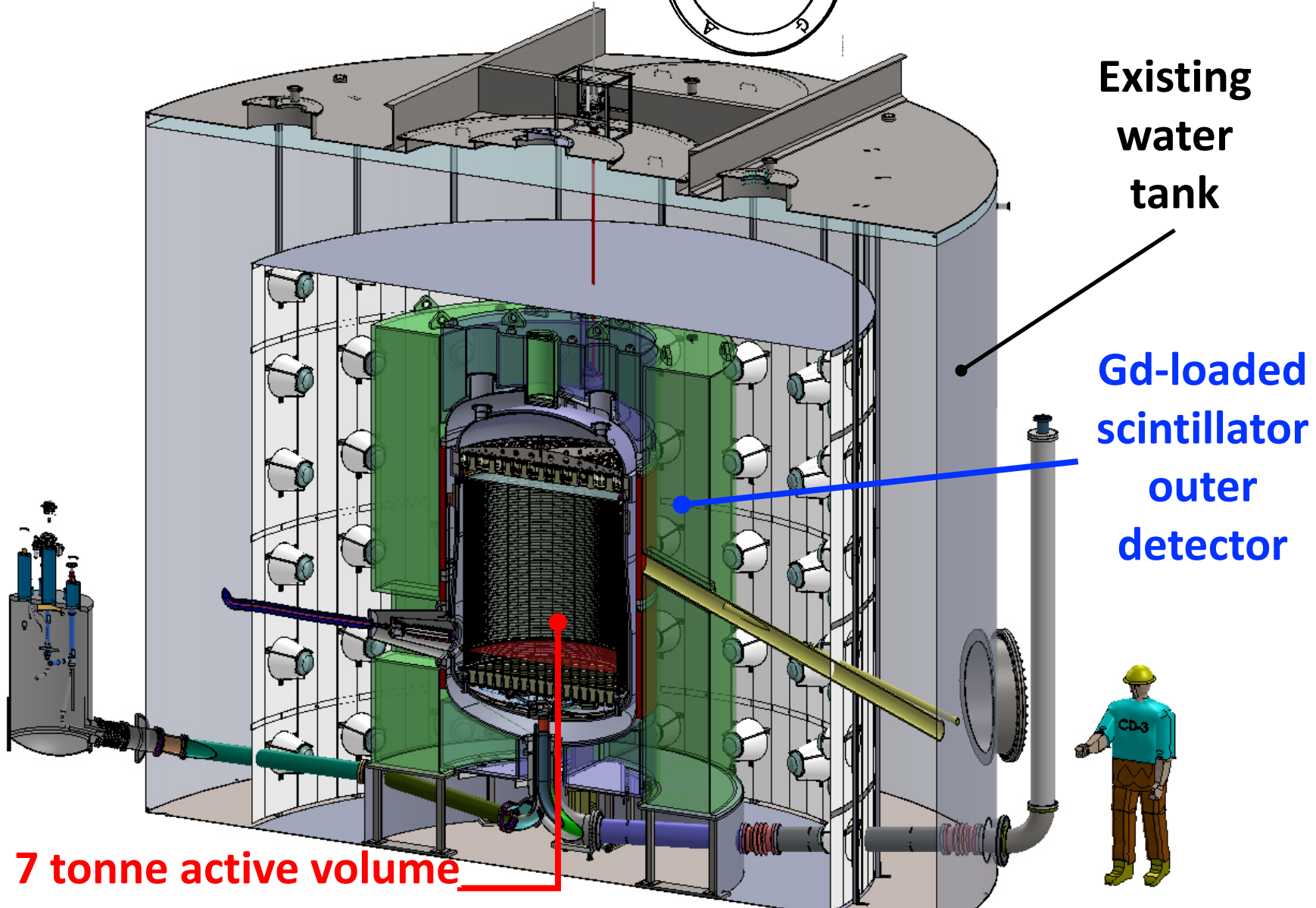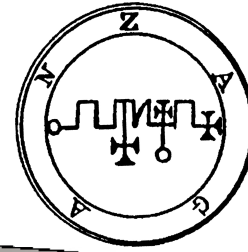
7 tonne active volume liquid Xe TPC; 10 tonnes total

Sneaky demons on the surfaces
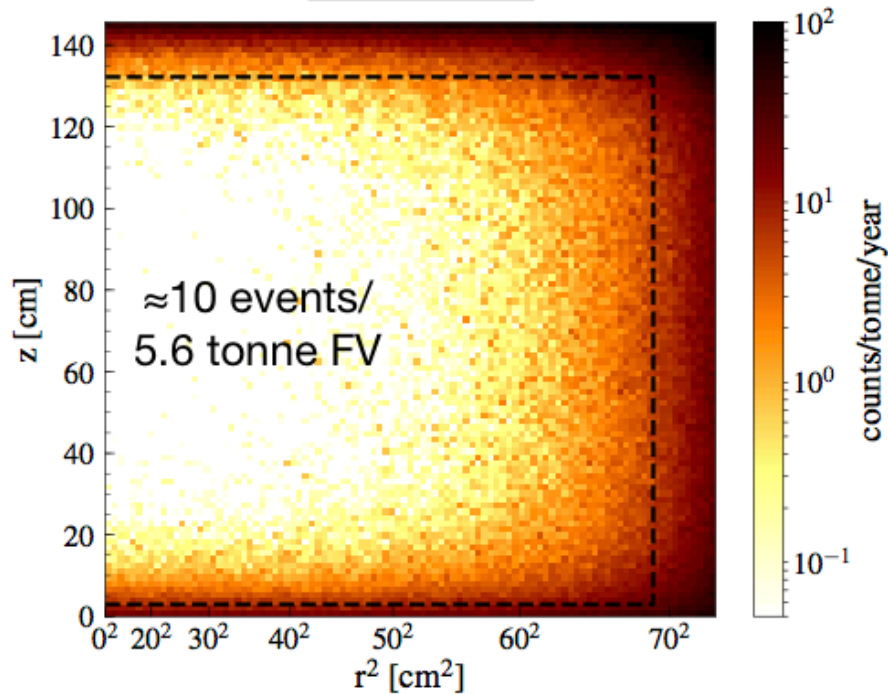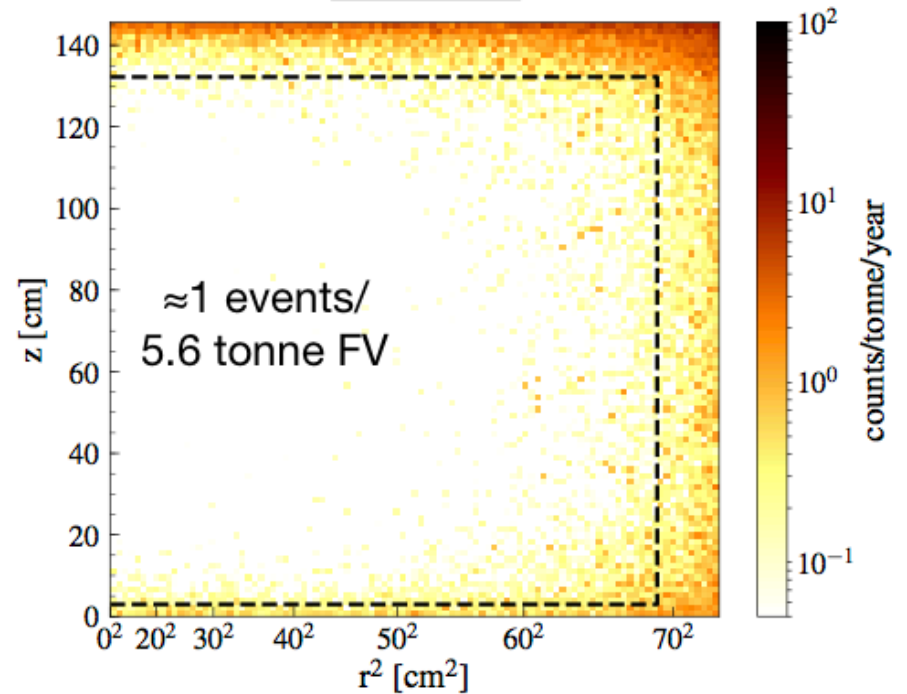
Outer Detectors Tag Background
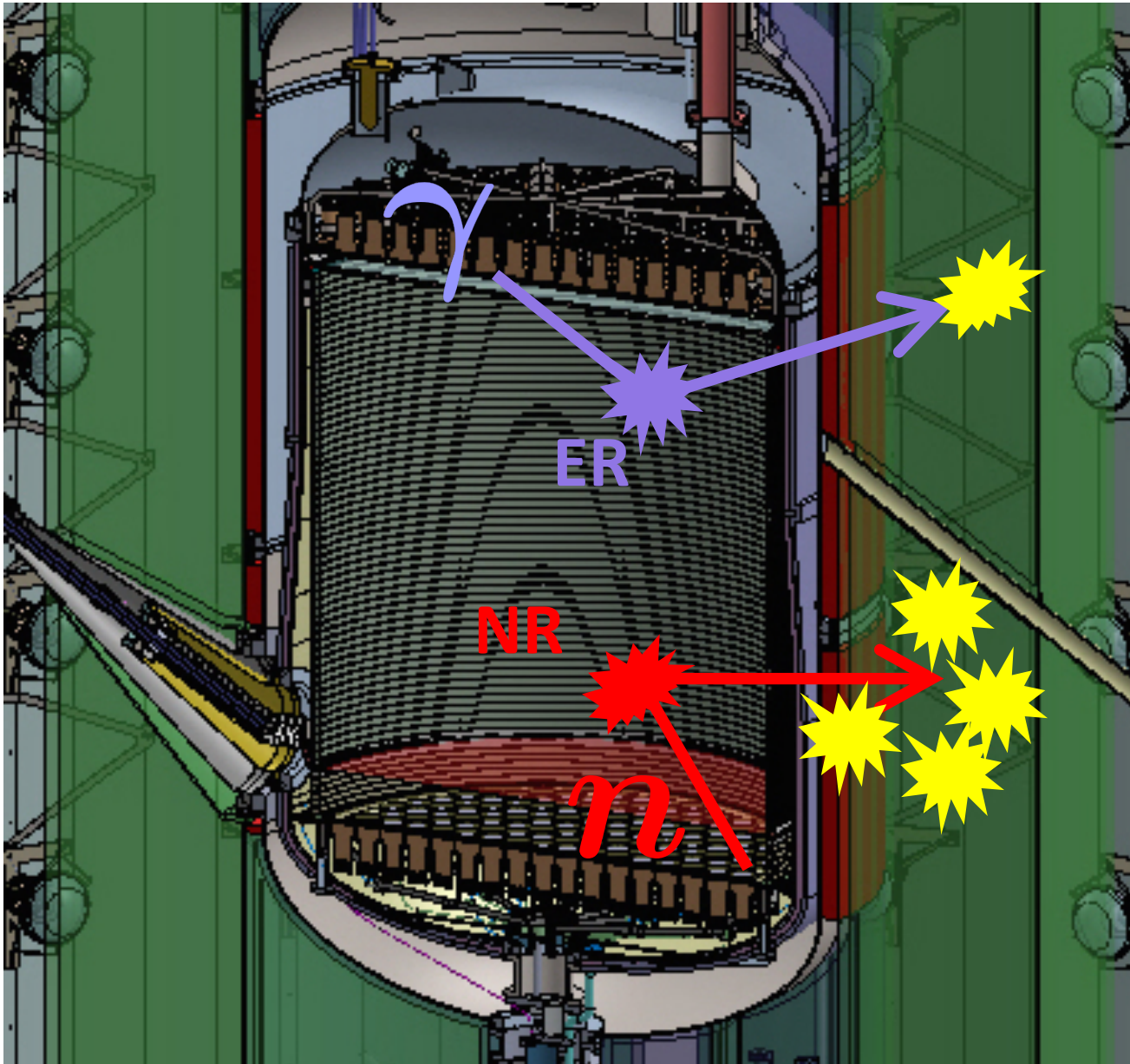
LZ Titanium Cryostat
super low background (Pawel Majewski)

- Fabrication complete at Loterios in Italy

Cryostat is at the lab in South Dakota!

LZ Low Radon Clean Room at Sanford Lab in South Dakota

- Low radon, class 100-1000 cleanroom ready at SURF for first parts
- Radon reduction system installed
- Underground improvements started, to finish by May

LZ titanium cryostat in that clean room

LZ Background table... tl;dr

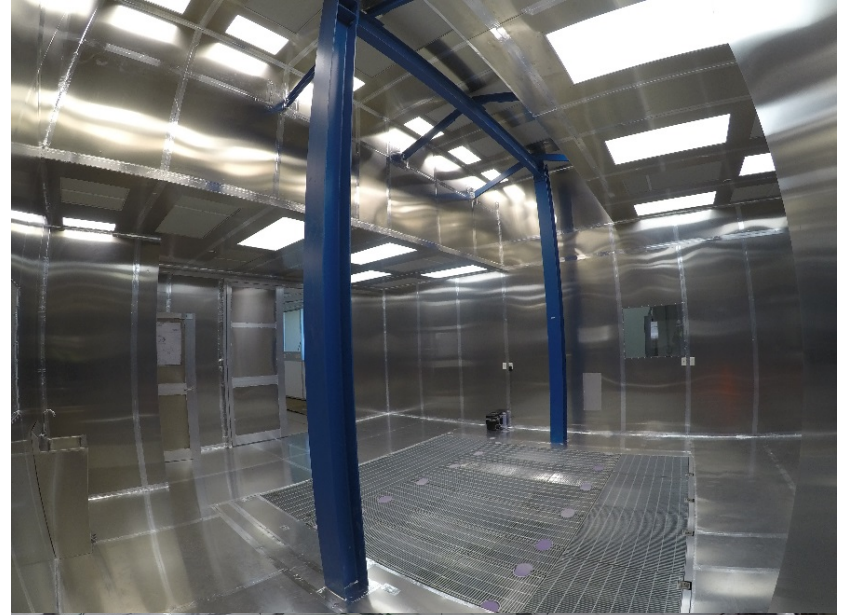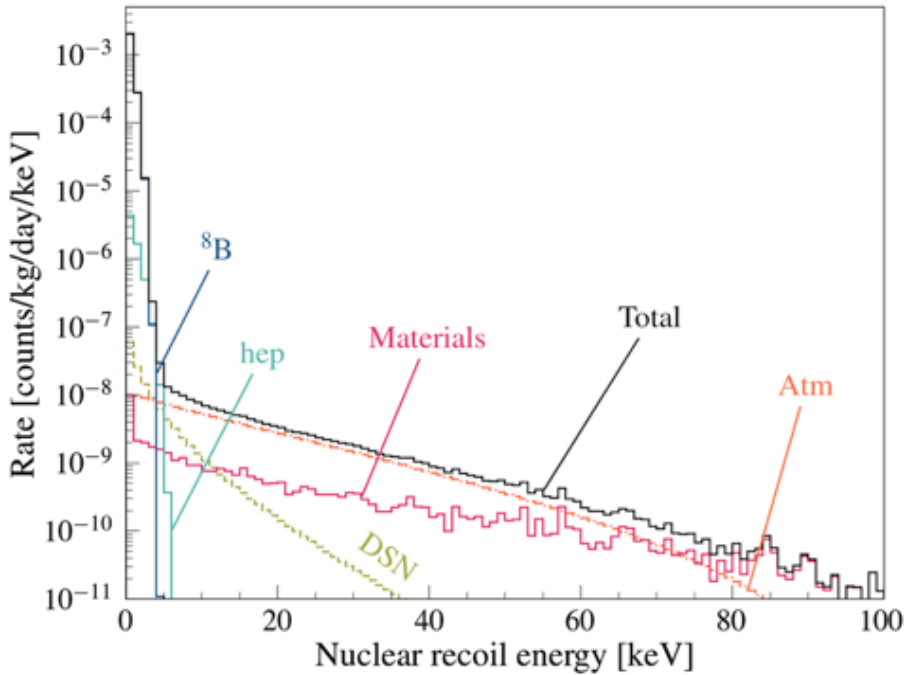|	Background Source	Mass (kg)	U early (mBq/kg)	U late (mBq/kg)	Th early (mBq/kg)	Th late (mBq/kg)	Co60 (mBq/kg)	K40 (mBq/kg)	n/yr	ER (cts)	NR (cts)
External Backgrounds	**Detector Components**									**9**	**0.07**
	PMT Structures	122	3.89	0.95	0.72	0.65	0.23	3.28	13.6	0.31	0.002
	R11410 3" PMTs	92	71.6	3.20	3.12	2.99	2.91	15.4	81.8	1.27	0.011
	R8778 2" PMTs	6	138	59.4	16.9	16.9	16.2	413	53.0	0.05	0.006
	R8520 Skin 1" PMTs	2	62.2	5.29	4.91	4.85	24.4	337	53.7	0.02	0.005
	PMT Bases	3	359	78.0	39.1	33.4	1.06	55.4	28.9	0.28	0.002
	PMT Cabling	83	6.19	7.06	1.34	1.67	0.01	6.45	17.5	0.89	0.001
	TPC PTFE	184	0.02	0.02	0.03	0.03	0.00	0.12	22.5	0.04	0.006
	Grid Wires and Rings	96	7.39	2.76	2.49	2.28	10.0	28.0	16.3	3.64	0.005
	Field Shaping Rings	92	5.49	1.14	0.72	0.65	0.00	2.00	41.0	0.65	0.011
	TPC Sensors and Thermometers	5	21.8	5.82	2.29	1.88	1.32	61.0	6.75	0.06	0.001
	PMT Conduits, HX and Tubing	215	3.18	0.46	0.46	0.56	1.23	1.39	5.87	0.03	0.001
	HV Conduits and Cables	138	3.61	2.30	0.61	0.76	1.4	2.5	26.5	0.02	0.001
	Cryostat	2778	2.88	0.63	0.48	0.51	0.31	2.62	323	1.27	0.018
	Outer Detector	22950	6.13	4.74	3.78	3.71	0.33	13.8	8061	0.62	0.001
	Surface Contamination									**40**	**0.39**
	Dust (intrinsic activity, 500 ng/cm2)									0.2	0.05
	Plate-out (PTFE panels, 50 nBq/cm2)									-	0.05
	210Bi mobility (0.1 µBq/kg)									40.0	-
	Ion-misreconstruction (50 nBq/cm2)									-	0.16
	210Pb (in bulk PTFE, 10 mBq/kg)									-	0.12
	Laboratory and Cosmogenics									**5**	**0.06**
	Laboratory Rock Walls									4.6	0.00
	Muon Induced Neutrons									-	0.06
	Cosmogenic Activation									0.2	-
Internal Backgrounds	**Xenon Contaminants**									**816**	**0**
	222Rn (1.81 µBq/kg)									678	-
	220Rn (0.09 µBq/kg)									111	-
	natKr (0.015 ppt g/g)									24.5	-
	natAr (0.45 ppb g/g)									2.5	-
	Physics									**322**	**0.51**
	136Xe 2νββ									67	0
	Solar neutrinos (pp+7Be+13N)									255	0
	Diffuse supernova neutrinos									0	0.05
	Atmospheric neutrinos									0	0.46
	Total									1192	1.03
	Total (with 99.5% ER discrimination, 50% NR efficiency)									5.96	0.51
											6.48

Surface devils – dust, radon daughters

Surface devils – getters, cables, plumbing

Surface devils – earth's atmosphere

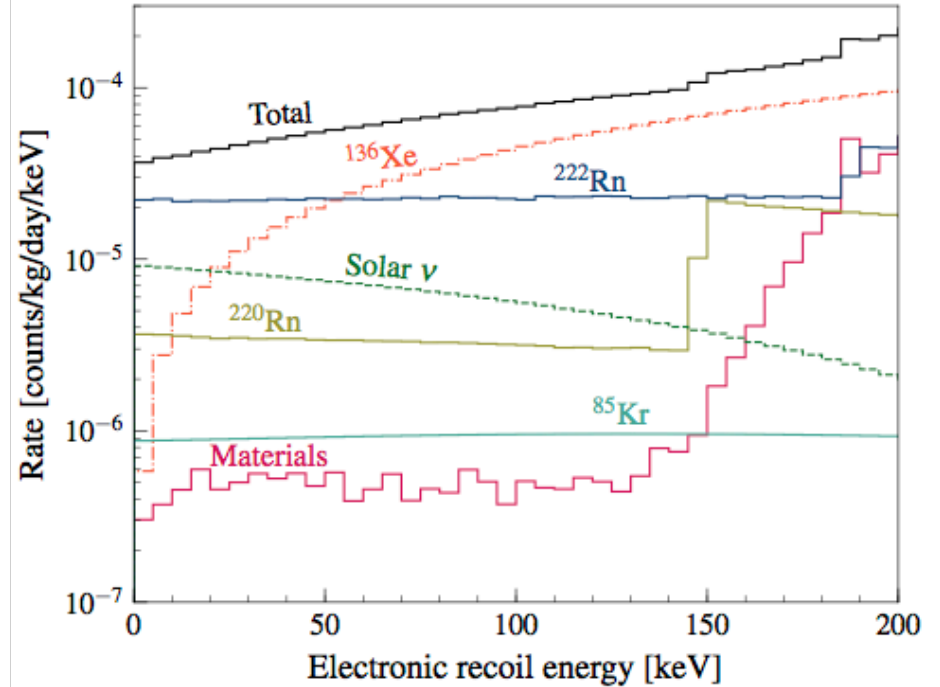# Plots of the expected LZ background

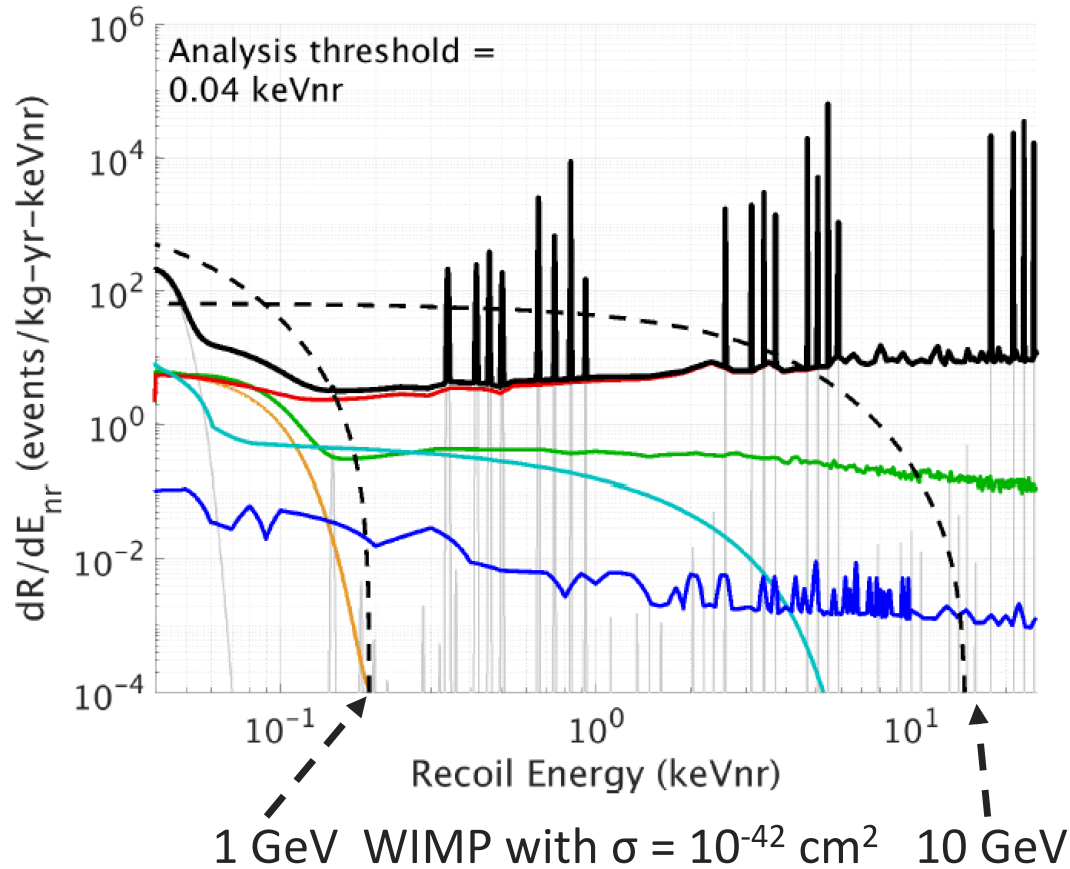from screening **measurement**s, physics calcs, simulations

Plot of the SCDMS background

Total
³H and Comptons   Ge activation   Surface betas   Surface ²⁰⁶Pb
neutrons   Coherent neutrinos

Ben Loer

ER Calibration: LUX CH$_3$T Injection

Electron Recoil (ER) **Background**

tritiated methane
(100,000's)

0.5 keV$_{ee}$ 1.7   2.9   4.2   5.4   6.6
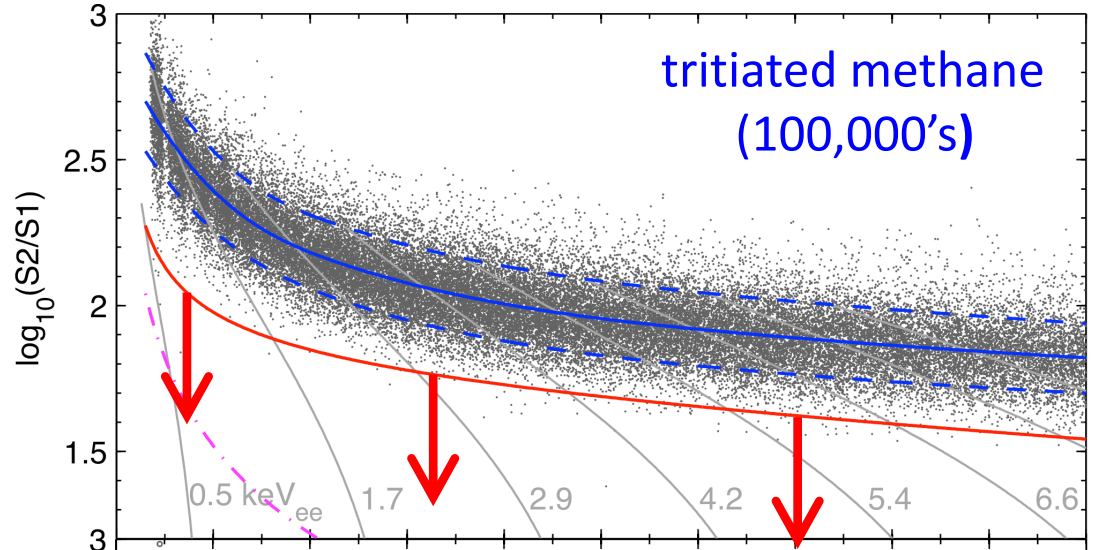
Nuclear Recoil (NR) **Signal**

9 keV$_{nr}$
15
21
27
33   39   45   51

DD neutrons

3 keV$_{nr}$

log$_{10}$(S2/S1)

S1 detected photons
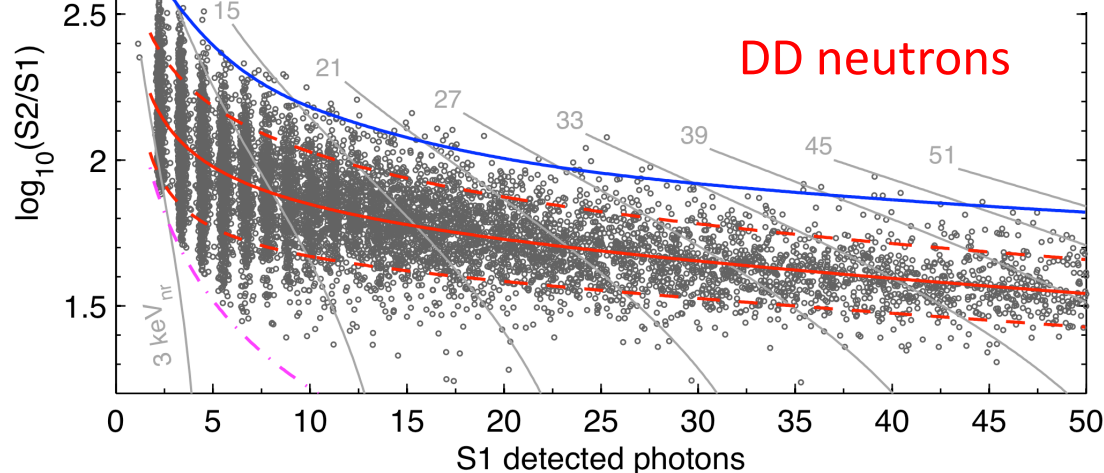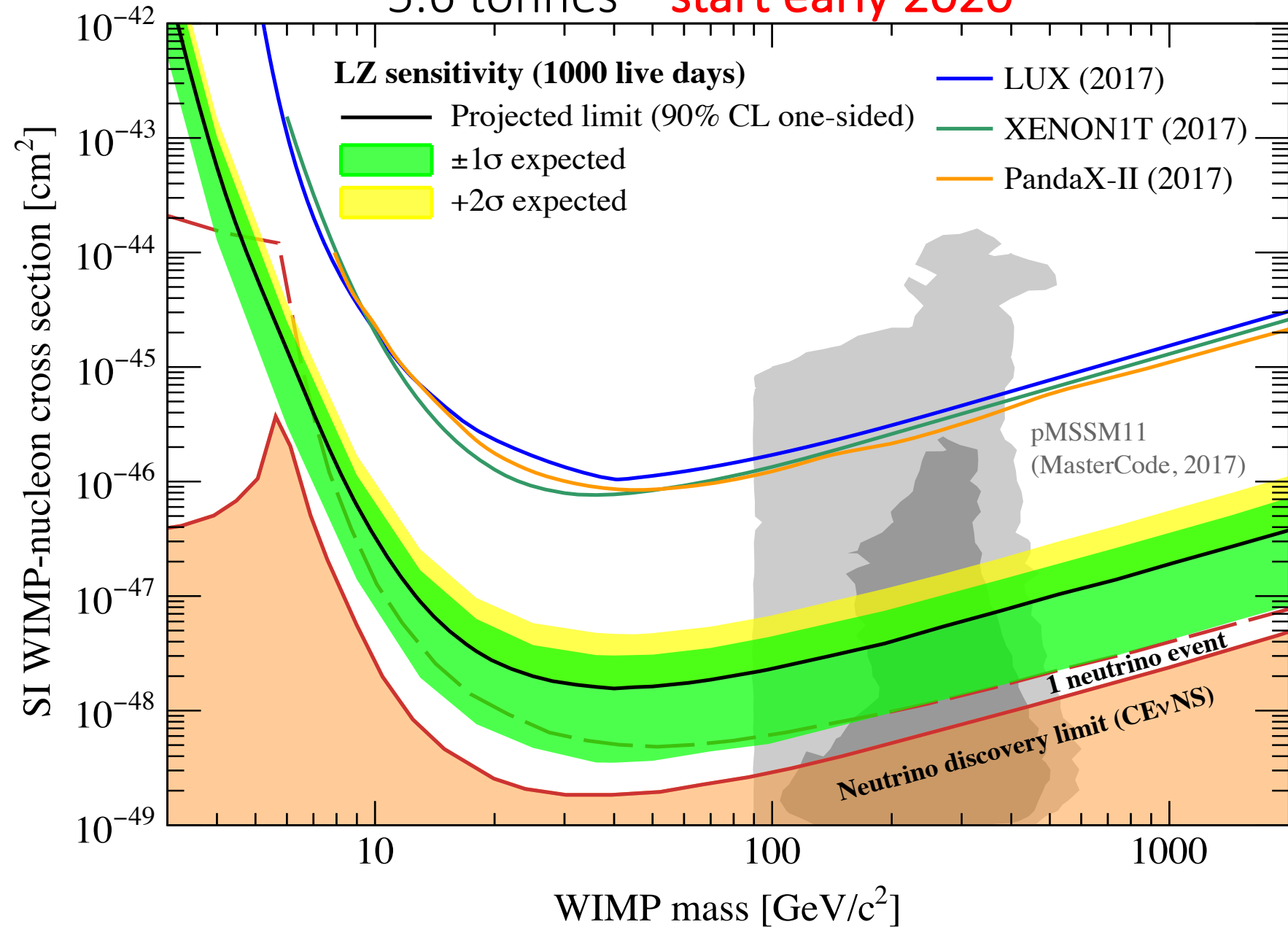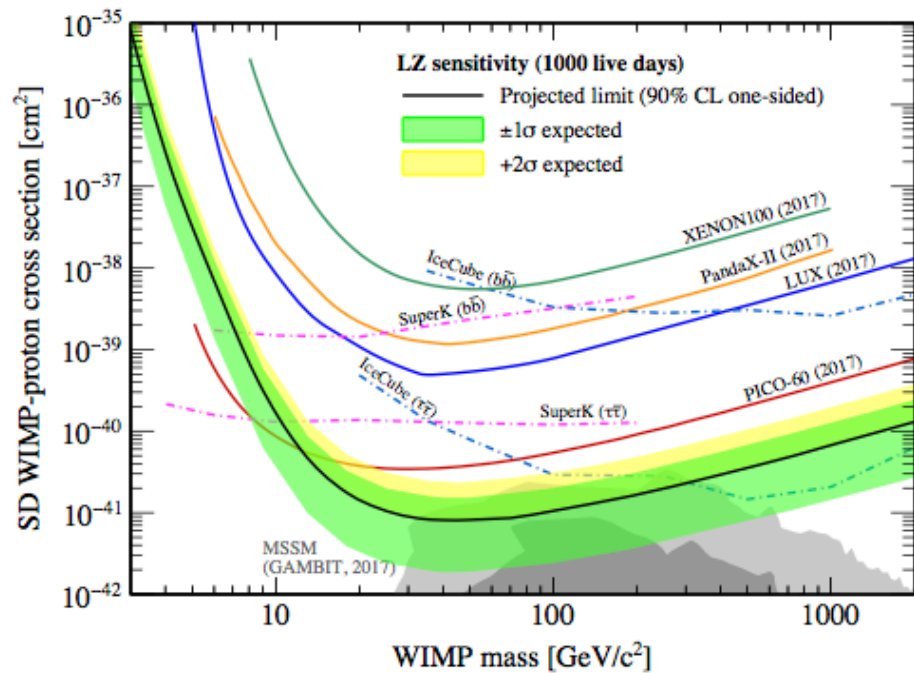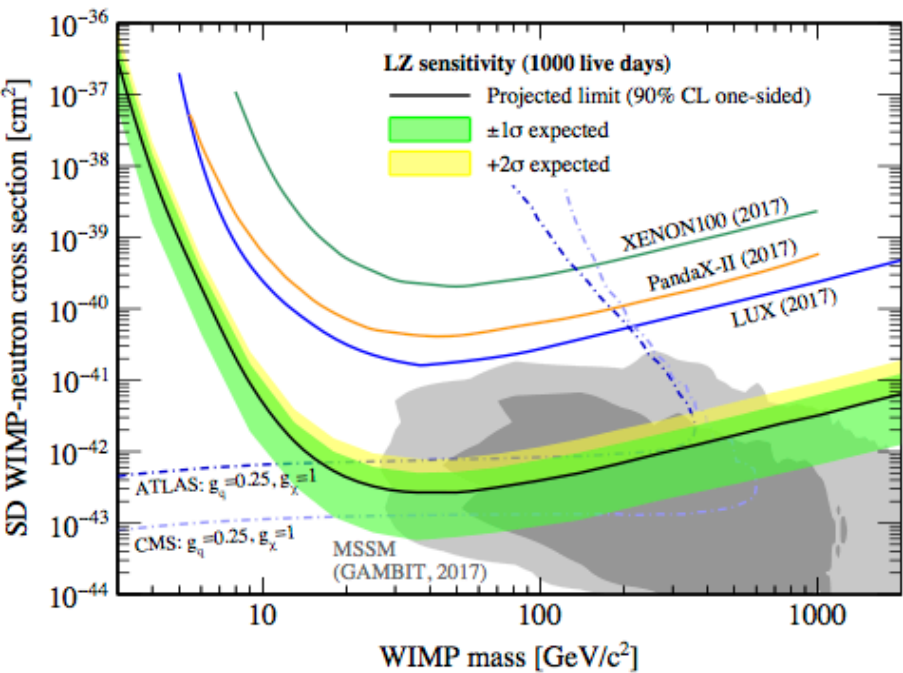
LZ Projected SI WIMP sensitivity

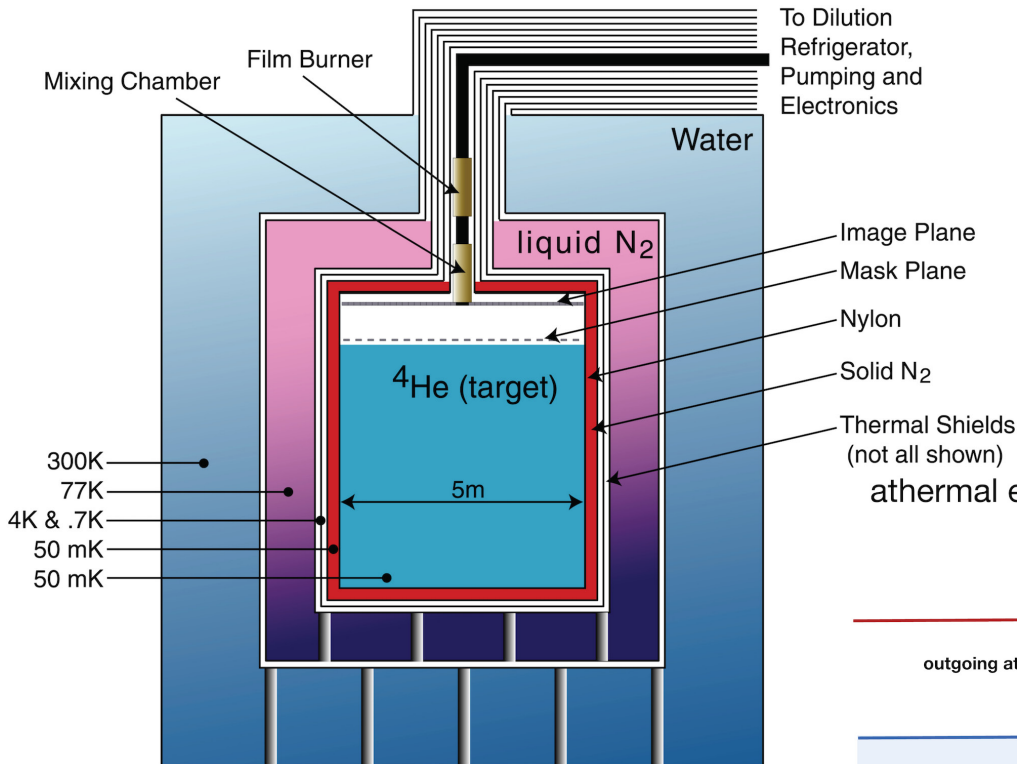## 5.6 tonnes – start early 2020

LZ Projected SD WIMP sensitivity
5.6 tonnes – start early 2020
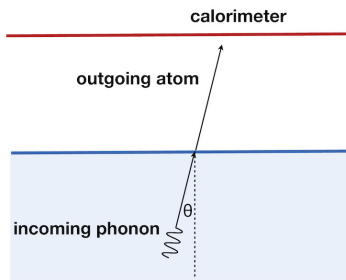
The LXe future (other than expansion)

- Dope with Helium or Neon
- Dope with CH_4
- Study/improve S2-only
- Further Suppress Radon etc
  Would love to deplete ^{136}Xe
  (cost requires $0\nu\beta\beta$
  cooperation, or, a detection)

Low energy/mass – Liquid Helium
(Bob Lanou... Dan McKinsey/Scott Hertel)

Mixing Chamber
Film Burner

To Dilution Refrigerator, Pumping and Electronics

Water

liquid N$_2$

Image Plane
Mask Plane
Nylon
Solid N$_2$
Thermal Shields (not all shown)

^{4}He (target)

5m

300K
77K
4K & .7K
50 mK
50 mK

20 tonnes. 2005

Energy Spectrum of the Excitations in Liquid Helium*

R. P. FEYNMAN AND MICHAEL COHEN
California Institute of Technology, Pasadena, California
(Received February 27, 1956)

A wave function previously used to represent an excitation (phonon or roton) in liquid helium, inserted into a variational principle for the energy, gave an energy-momentum curve having the qualitative shape suggested by Landau; but the value computed for the minimum energy Δ of a roton was 19.1°K, while thermodynamic data require Δ=9.6°K. A new wave function is proposed here. The new value computed for Δ is 11.5°K. Qualitatively, the wave function suggests that the roton is a kind of quantum-mechanical analog of a microscopic vortex ring, of diameter about equal to the atomic spacing. A forward motion of single atoms through the center of the ring is accompanied by a dipole distribution of returning flow far from the ring.

In the computation both the two-atom and three-atom correlation functions appear. The former is known from x-rays, while for the latter the Kirkwood approximation of a product of three two-atom correlation functions is used. A method is developed to estimate and correct for most of the error caused by this approximation, so that the residual uncertainty due to this source is negligible.

athermal evaporation

calorimeter

outgoing atom

θ

incoming phonon

chance per interaction high: ~25%
-> nearly all phonon/roton energy
will end up as athermal evaporation

Energy [meV]
1.6
1.2
0.8
0.4
0.0

Critical Angle [degrees]
80
70
60
50
40
30
20
10

Phonons
R-
Rotons R+
Binding Energy
Critical Angle
evap.

0   1   2   3
Wave Vector [Å^{-1}]
(momentum)